Appendix J THM-coupled simulation of a compacting backfilled drift

Table of content

1 Objective and scope

In order to investigate whether the material models for crushed salt implemented in CODE_BRIGHT are in principle applicable for simulating the in-situ behaviour of a backfilled drift, a simplified drift model was developed, and several model variants involving the backfill evolution under dry conditions and with brine inflow, at ambient and elevated temperature, were simulated.

The objective of these simulations was to test the capabilities of the implemented models, especially with coupling of mechanical, hydraulic and thermal effects, in a system involving the crushed salt backfill and the surrounding rock salt. To perform a reliable prediction of the backfill evolution in a realistic repository system was not the aim. Therefore, several simplifications regarding geometry and boundary conditions introduced and explained further down were considered acceptable.

2 Model description

2.1 Geometrical model

For the simulations an axial-symmetric model of 80 m length and 100 m radius was used, with the axis in the direction of the drift (Fig. 2.1). Consequently, the drift has a circular cross section, the drift radius amounts to 2.9 m. The surrounding rock salt is divided into rock mass, near field and excavation-damaged zone (EDZ). These are modelled essentially in the same way, although the EDZ features a somewhat higher porosity (see next section). 65 m of drift length (left hand side in Fig. 2.1) are backfilled with crushed salt, while a concrete plug is installed drift in the right 15 m of the model. The EDZ has been removed in the plug region.

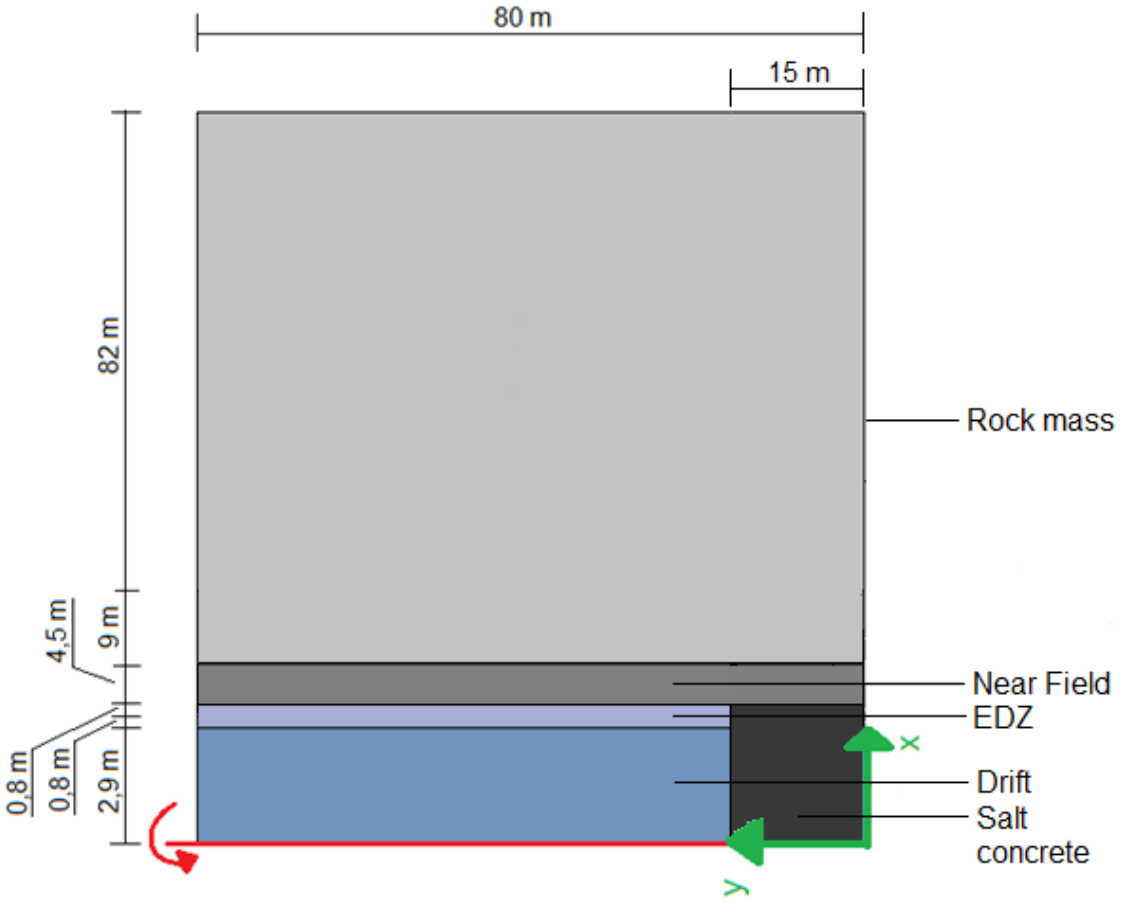

Fig. 2.1 Overview of the model geometry

2.2 Physical model and constitutive laws

The model for mechanical behaviour of the crushed salt includes the following mechanisms:

- elastic deformation
- dislocation creep
- viscoplasticity for granular material representing grain reorganisation and breaking
- fluid assisted diffusional transfer
- thermal expansion (for non-isothermal simulations)

The various contributions are combined by adding the individual deformation rates. A description of the formulations is given further down.

For rock salt, only elasticity, dislocation creep and thermal expansion are considered. The EDZ is modelled with the same parameters as the undisturbed rock, except for an increased porosity (3% instead of 1%). The idea is to slightly moderate the sharp porosity contrast to the backfill (initially 29.77%). Dilatancy evolution of the EDZ is not considered, because the work is focused on backfill performance (although a respective approach is available in CODE_BRIGHT). Like rock salt, salt concrete is modelled with elasticity, dislocation creep and thermal expansion, but with different parameters.

The hydraulic behaviour of the materials is described by their intrinsic permeabilities, van Genuchten type retention curve and relative permeabilities, and diffusive fluxes of vapour and dissolved salt. The simulations consider partially saturated systems and run at most until full saturation of the backfill, therefore positive pore pressures do not occur.

Heat transfer is restricted to conductive flux of heat in the non-isothermal simulation. For thermal-mechanical coupling linear thermal expansion of solid and liquid phases is considered.

In the following sections, the constitutive laws applied are described.

2.2.1 Mechanical behaviour

In CODE_BRIGHT the deformation ratio is calculated as the sum of different contributions:

$$\dot{\varepsilon}_{CS} = \dot{\varepsilon}^{EL} + \dot{\varepsilon}^{DC} + \dot{\varepsilon}^{VP} + \dot{\varepsilon}^{FADT} + \dot{\varepsilon}^{TH} \quad (1)$$

(EL = linear elasticity, DC = dislocation creep, VP = viscoplasticity for granular materials, FADT = fluid assisted diffusional transfer, TH = thermal influence) /COD 10/. The individual contributions are explained in the following sections.

2.2.1.1 Linear elasticity

This law describes the elastic behaviour of the material. An isotropic approach is chosen because a statistic orientation of the grains is assumed. Following Hooke´s law, in CODE_BRIGHT linear elasticity is described using two independent variables, Young's

modulus E and Poisson´s ratio ν. Young's modulus shows a linear dependence on porosity according to

$$E = E_0 + (\eta - \eta_0)\frac{dE}{d\eta} \tag{2}$$

(E = Young's modulus, dE/dη = variation of Young's modulus with porosity, η_0 = reference porosity). η_0 and E_0 are given constants /COD 10/.

2.2.1.2 Dislocation creep

This law describes the dislocation creep which is a time dependent deformation mechanism. CODE_BRIGHT uses a modification which enables a creep compaction for materials with a significant porosity /COD 10/. For stationary conditions the equation is

$$\dot{\varepsilon}_{ij}^{DC} = \frac{1}{\mu_{dev}^{DC}} \cdot \Phi(F) \cdot \frac{\partial G}{\partial \sigma'} \tag{3}$$

$\Phi(F) = F^n$ is a scalar function with n = stress exponent, F = function of stress and G = flow rule.

The flow rule and the function of stress are defined as

$$G = F = \sqrt{q^2 + \left(\frac{-p'}{\alpha_p}\right)^2} \tag{4}$$

Here q is the deviatoric stress and p' is the mean normal stress. α_p is a material parameter and defined as

$$\alpha_p = \left(\frac{\mu_{vol}^{DC}}{\mu_{dev}^{DC}}\right)^{1/(n+1)} \tag{5}$$

μ_{dev} is the deviatoric viscosity, μ_{vol} is the volumetric viscosity and both are dependent on the void ratio e:

$$\frac{1}{\mu_{dev}^{DC}} = A(T) \cdot g_{dev}^{DC}(e) \qquad \frac{1}{\mu_{vol}^{DC}} = A(T) \cdot g_{vol}^{DC}(e) \tag{6) + (7)}$$

The dependence on temperature is described by the structural parameter A_A, the activation energy Q_B, the general gas constant R and the absolute temperature T:

$$A(T) = A_A \cdot \exp(\frac{-Q_A}{R \cdot T}) \tag{8}$$

The functions of the void ratio are described by

$$g_{vol}^{DC}(e) = 3 \cdot (g-1)^n \cdot f \tag{9}$$

$$g_{dev}^{DC}(e) = \left(\sqrt{\frac{1+g+g^2}{3}} \right)^{n-1} \cdot \left(\frac{2 \cdot g + 1}{3} \right) \cdot f + \frac{1}{\sqrt{g}} \tag{10}$$

where g and f are given by

$$g = \frac{1}{(1-f)^2} \qquad f = \sqrt{\frac{2e}{3 \cdot (1-e^{3/2}) \cdot (1+e)}} \tag{11) + (12)}$$

2.2.1.3 Viscoplasticity for granular materials

This is a general model for soils to describe the viscoplasticity and the plastic behaviour of the bond between the grains:

$$\dot{\varepsilon}_{ij}^{VP} = \Gamma \cdot < \Phi(F) > \frac{\partial G}{\partial \sigma} \tag{13}$$

where $\Phi(F) = F^m$ for $F > 0$ otherwise $\Phi(F) = 0$ (14)

The flow rule and the yield function for crushed salt are defined by

$$G = F = q^2 - \delta^2 (p_0 \cdot p' - p'^2) \tag{15}$$

with the deviatoric stress q, the mean normal stress p' and a parameter δ.

The temperature-dependent viscosity is given by

$$\Gamma = \Gamma_0 \cdot \exp(\frac{-Q}{R \cdot T}) \tag{16}$$

Here Γ_0 is a scaling factor, Q is the activation energy, R is the gas constant and T is the temperature.

Strain hardening of the material is achieved by a change of the pressure p_0 with the volumetric deformation ε_V. D and l are parameters.

$$dp_0 = D \cdot l \cdot \varepsilon_V^{l-1} \cdot d\varepsilon_V \tag{17}$$

The formulation G = F does not permit a volume increase. This restriction is acceptable for the description of crushed salt.

2.2.1.4 Viscoelasticity for Saline Materials (FADT)

The deformation mechanism fluid assisted diffusional transfer (FADT) was introduced to describe the influence of liquid on deformation behaviour. The deformation rate is linear and stress dependent:

$$\dot{\varepsilon}_{ij}^{FADT} = \frac{1}{2\mu_{dev}^{FADT}}(\sigma'_{ij} - p' \cdot \delta_{ij}) + \frac{1}{3\mu_{vol}^{FADT}} p' \cdot \delta_{ij} \tag{18}$$

μ_{dev} is the deviatoric viscosity, μ_{vol} is the volumetric viscosity and δ_{ij} is the Kronecker symbol.

The volumetric viscosity and the deviatoric viscosity are described by

$$\frac{1}{\mu_{vol}^{FADT}} = \frac{16B(T)\sqrt{S_l}}{d_0^3} g_{vol}^{FADT}(e) \qquad \frac{1}{2\mu_{dev}^{FADT}} = \frac{16B(T)\sqrt{S_l}}{d_0^3} g_{dev}^{FADT}(e) \tag{19) + (20}$$

The viscosities are dependent on the degree of saturation (S_l), the grain size (d_0) and functions of temperature and void ratio.

$$B(T) = \frac{A_B}{R \cdot T} \cdot \exp(\frac{Q_B}{R \cdot T}) \tag{21}$$

captures the dependence on the temperature and contains the pre-exponential parameter A_B, the activation energy Q_B, the general gas constant R and the temperature T.

$$g_{vol}^{FADT}(e) = \frac{3g^2 \cdot e^{3/2}}{1+e} \text{ and } g_{dev}^{FADT}(e) = \frac{g^2}{1+e} \tag{22) + (23}$$

capture the dependence on the void ratio e. The functions g and f are defined as in equation (11) and (12).

2.2.1.5 Thermal expansion

Thermal expansion is described by

$$\dot{\varepsilon}ij^{TH} = 3b_S \Delta T \tag{24}$$

(b_s = Linear thermal expansion coefficient of the material)

2.2.2 Hydraulic behaviour

For the hydraulic behaviour it is assumed that the liquid and gas flows follow Darcy's law, with the actual effective permeability to each phase being given by the product of intrinsic and relative permeability. The dependence of intrinsic permeability k on porosity ϕ is given by

$$\mathrm{k} = \mathbf{k}_0 \cdot \frac{\phi^3}{(1-\phi)^2} \cdot \frac{(1-\phi_0)^2}{\phi_0^3} \tag{25}$$

with initial values k_0 and ϕ_0. The relative permeabilities of the liquid and gaseous phases are dependent on the degree of liquid saturation according to

$$\mathrm{S_e} = \frac{\mathrm{S_l} - \mathrm{S_{lr}}}{\mathrm{S_{ls}} - \mathrm{S_{lr}}} \qquad \mathrm{k_{rl}} = \mathrm{A} \cdot \mathrm{S_e^{\lambda}} \qquad \mathrm{k_{rg}} = 1 - \mathrm{k_{rl}} \tag{26) + (27) + (28}$$

where S_l, S_{lr}, S_{ls}, S_e are the actual, residual, maximum and effective saturation of liquid, respectively, and A and λ are parameters. It is necessary to define the retention curve of the materials relating the degree of saturation to suction. Generally, the formulation of van Genuchten with material parameters β, P_0 and σ_0 is selected.

$$S_e = \left[1 + \left(\frac{P_g - P_l}{P}\right)^{1/(1-\beta)}\right]^{-\beta} \quad \text{where} \quad P_g - P_l \geq 0 \quad \text{and} \quad P = P_0 \cdot \frac{\sigma}{\sigma_0} \tag{29}$$

P_0 is the pressure measured at a certain temperature, and σ_0 is the related surface tension.

The molecular diffusion of vapour is governed by Fick's law, a constant dispersion co-efficient corresponding to the molecular diffusion of vapour in air is assumed.

$$D_m^w = \tau D \left(\frac{(273.15 + T)^n}{P_g}\right) \tag{30}$$

where P_g is given in MPa. For the tortuosity τ a value of 1.0, for n a value of 2.3 and for D a value of 5.9E-6 m²/s were adopted.

2.2.3 Thermal behaviour

Heat transfer is restricted to conductive flux of heat following Fourier's law. Thermal conductivity is dependent on conductivities of the dry material and of the pore fluids, and on porosity. The effective thermal conductivity is calculated as the geometric weighted mean for the dry or the saturated case:

$$\lambda_{dry} = \lambda_{solid}^{(1-\phi)} \cdot \lambda_{gas}^{\phi} \qquad \lambda_{sat} = \lambda_{solid}^{(1-\phi)} \cdot \lambda_{liq}^{\phi} \tag{31) + (32}$$

The thermal conductivity of the solid salt fraction is dependent on temperature. This is approximated by a polynomial:

$$\lambda_{solid} = (\lambda_{solid})_0 + a_1 T + a_2 T^2 + a_3 T^3 \tag{33}$$

In the drift simulation, however, thermal conductivity of air or water in the pore space was neglected, so that only the solid thermal conductivity contributed to heat transfer.

2.3 Material data

2.3.1 Rock salt

Linear elasticity		
E	10000	MPa
dE/dΦ	0	MPa
v	0.18	-
Φ_0	0.1	-
Φ_{min}	0.1	-
E_{min}	0	MPa

Thermal expansion		
b_s	4.20E-05	$°C^{-1}$

Dislocation creep		
A_A	1.04E-06	$s^{-1}MPa^{-n}$
Q_A	5.40E+04	J mol^{-1}
n	5.00	-

Retention curve		
P_0	0.01	MPa
$б_0$	0.072	Nm^{-1}
λ	0.37	-
S_{rl}	0.01	-
S_{ls}	1	-

Instrinsic permeability		
$(k_{11})_0$	1.00E-11	m^2
$(k_{22})_0$	1.00E-11	m^2
$(k_{33})_0$	1.00E-11	m^2
Φ_0	0.01	-
Φ_{min}	0.01	-

Liquid phase relative permeability		
A	1	-
λ	3	-
S_{rl}	0.01	-
S_{ls}	1	-

Gas phase relative permeability		
S_{rg}	0.99	-

Diffusive flux of vapour		
D	5.9 E-6	$M^2s^{-1}K^{-n}Pa$
N	2.3	-
τ_0	1	-
m	0	-

Diffusive flux of dissolved salt and air		
D	1.1 E-4	$m^2\,s^{-1}$
Q	24530	J mol^{-1}
τ	1	-

Conductive flux of heat		
$(\lambda_{solid})_0$	6.1	W mK^{-1}
λ_{Gas}	1	W mK^{-1}
λ_{liq}	1	-
a_1	-2.43E-2	-
a_2	-5.8E-5	-
a_3	-5.5E-8	-
Solid phase properties		
C_s	855	J kg^{-1} K^{-1}
ρ_s	2160	kg m^{-3}
α_s	4.2E-5	$°C^{-1}$
T_0	29	°C
Liquid phase properties		
ρ_{lo}	1025	kg m^{-3}
β	4.5E-4	MPa^{-1}
α	-4.2E-4	$°C^{-1}$
γ	0.1	-

2.3.2 Crushed salt backfill

Linear elasticity		
E	1.0	MPa
dE/dΦ	-4.00E+3	MPa
v	0.27	-
Φ_0	0.2977	-
Φ_{min}	0.1	-
E_{min}	0	MPa
Thermal expansion		
b_s	2.90E-04	$°C^{-1}$
Fluid assisted diffusional transfer		
d_0	4.00E-04	m
A_B	3.00E-13	s^{-1} MPa^{-1} m^3
Q_B	24530	J mol^{-1}
Dislocation creep		
A_A	2.08E-08	$s^{-1}MPa^{-n}$
Q_A	5.40E+04	J mol^{-1}
n	5.00	-
Viscoplastic deformation behaviour of granular material		
δ	10.00	-
Γ_0	7.00E-05	s^{-1}
Q	5.40E+04	J mol^{-1}
p_0	0.10	MPa
D	1.00E+04	MPa
l	4.00	-
Retention curve		
P_0	0.01	MPa
$б_0$	0.072	Nm^{-1}
λ	0.37	-
S_{rl}	0.01	-
S_{ls}	1	-

Instrinsic permeability

$(k_{11})_0$	1.00E-11	m^2
$(k_{22})_0$	1.00E-11	m^2
$(k_{33})_0$	1.00E-11	m^2
Φ_0	0.28	-
Φ_{min}	0.01	-

Liquid phase relative permeability

A	1	-
λ	3	-
S_{rl}	0.01	-
S_{ls}	1	-

Gas phase relative permeability

S_{rg}	0.99	-

Diffusive flux of vapour

D	5.9 E-6	$M^2s^{-1}K^{-n}Pa$
N	2.3	-
τ_0	1	-
m	0	-

Diffusive flux of dissolved salt and air

D	1.1 E-4	$m^2\ s^{-1}$
Q	24530	$J\ mol^{-1}$
τ	1	-

Conductive flux of heat

$(\lambda_{solid})_0$	6.1	$W\ mK^{-1}$
λ_{Gas}	1	$W\ mK^{-1}$
λ_{liq}	1	-
a_1	-2.43E-2	-
a_2	-5.8E-5	-
a_3	-5.5E-8	-

Solid phase properties

C_s	855	$J\ kg^{-1}\ K^{-1}$
ρ_s	2160	$kg\ m^{-3}$
α_s	4.2E-5	$°C^{-1}$
T_0	29	°C

Liquid phase properties

ρ_{lo}	1025	$kg\ m^{-3}$
β	4.5E-4	MPa^{-1}
α	-4.2E-4	$°C^{-1}$
γ	0.1	-

2.3.3 Salt concrete plug

Linear Elasticity

E	25000	MPa
dE/dΦ	0	MPa
v	0.18	-
Φ_0	0.06	-
Φ_{min}	0.01	-
E_{min}	0	MPa

Thermal expansion

b_s	4.20E-05	$°C^{-1}$

Dislocation creep

A_A	1.04E-06	$s^{-1}MPa^{-n}$
Q_A	5.40E+04	J mol^{-1}
n	5.00	-

Retention Curve

P_0	0.01	MPa
$б_0$	0.072	Nm^{-1}
λ	0.37	-
S_{rl}	0.01	-
S_{ls}	1	-

Instrinsic Permeability

$(k_{11})_0$	1.00E-18	m^2
$(k_{22})_0$	1.00E-18	m^2
$(k_{33})_0$	1.00E-18	m^2
$Φ_0$	0.01	-
$Φ_{min}$	0.01	-

Liquid Phase Relative Permeability

A	1	-
λ	3	-
S_{rl}	0.01	-
S_{ls}	1	-

Gas Phase Relative Permeability

S_{rg}	0.99	-

Diffusive Flux of Vapour

D	5.9 E-6	$M^2s^{-1}K^{-n}Pa$
N	2.3	-
$τ_0$	1	-
m	0	-

Diffusive Flux of Dissolved Salt and Air

D	1.1 E-4	$m^2\ s^{-1}$
Q	24530	J mol^{-1}
τ	1	-

Conductive Flux of Heat

$(λ_{solid})_0$	5.73	W mK^{-1}
$λ_{Gas}$	1	W mK^{-1}
$λ_{liq}$	1	-
a_1	-1.84E-2	-
a_2	-2.86E-5	-
a_3	-1.51E-8	-

Solid Phase Properties

C_s	855	J kg^{-1} K^{-1}
$ρ_s$	2200	kg m^{-3}
$α_s$	4.2E-5	$°C^{-1}$
T_0	38.67	°C

Liquid Phase Properties

$ρ_{lo}$	1002.6	kg m^{-3}
β	4.5E-4	MPa^{-1}
α	-3.4E-4	$°C^{-1}$
γ	0.6923	
P_{l0}	0.01	MPa

2.4 Simulation variants, schedule, and boundary conditions

Three simulation variants were performed and analysed:

- A coupled hydro-mechanical (HM) simulation at ambient temperature (38.67 °C), relevant for backfilled drifts far from waste disposal areas
- A coupled HM simulation at elevated temperature (60 °C), more relevant for drifts closer to disposal areas
- A coupled thermal-hydro-mechanical (THM) simulation with an axial temperature gradient

All variants featured a period of 100 years of drift convergence and backfill compaction under dry conditions and a subsequent brine inflow from the open drift side (left hand in Fig. 2.1), resulting in an accelerated backfill compaction. Each simulation was continued until a residual backfill porosity of 1 % was reached.

In the following, the initial and boundary conditions of the simulation cases are discussed in detail.

2.4.1 HM simulation at ambient temperature

The initial conditions of the first isothermal calculation are shown in Fig. 2.2 (left). The drift axis is the rotation axis, at the left and right hand sides of the model horizontal displacement is prevented, and a radial load of 18.67 MPa is applied circumferentially. Because of the axial symmetry, gravity has to be neglected in the model. Initial mechanical stress is 18.67 MPa isotropic, and the temperature is kept constant at 38.67 °C. These conditions are considered representative for the 850-m level of a repository. An initial suction of -10 MPa is applied in the entire model, corresponding to a saturation of 2.7 % of the rock.

At simulation start-up, the drift is excavated and the stress inside is set to -0.1 MPa (air pressure). Additionally, the EDZ is created and the salt concrete plug is emplaced. The drift is kept open for one year, afterwards it is backfilled instantly with crushed salt, again with a saturation of 2.7 % (-10 MPa suction). The initial porosities of the materials are 0.01 (rock salt), 0.03 (EDZ), 0.06 (plug), and 0.2977 (backfill). In Tab. 2.1, these data are summarised.

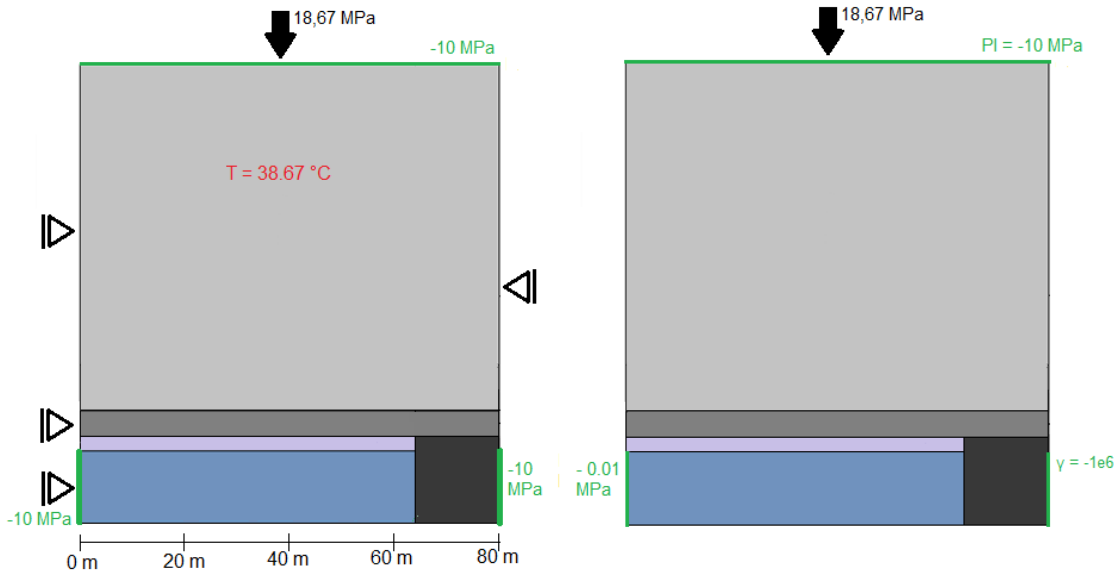

Fig. 2.2 Boundary conditions for the simulation at ambient temperature – left: initial conditions, right: change of boundary condition after 101 years simulation time

Tab. 2.1 Conditions of the simulation at ambient temperature after backfilling of the drift

	Drift	EDZ	Near field and rock	Salt concrete
Porosity	0.2977	0.03	0.01	0.06
Stress	-0.1 MPa	-18.67 MPa		
Liquid Pressure	-10.0 MPa			
Temperature	38.67°C			

After 100 years of convergence at dry conditions, the suction condition at the open drift side (Fig. 2.2, right hand) is changed to -0.01 MPa, which corresponds to a backfill saturation of 25 %. This is done in order to simulate a re-saturation of the crushed salt from the left side. At the same time, the mechanism of fluid-assisted diffusional transfer is activated in the backfill, and a seepage condition is applied to the right end of the salt concrete plug.

In the following simulation, the backfill is saturated from the left side of the model. Moreover, saturation additionally increases by the accelerated re-compaction of the backfill. The simulation runs until a residual porosity of 1% in the backfill is reached.

2.4.2 HM simulation at 60 °C

The isothermal calculation at 60 °C is run under exactly the same conditions as the one at ambient temperature, except for the elevated temperature. All other conditions discussed in the previous section and shown in Fig. 2.2 and Tab. 2.1 apply.

2.4.3 THM simulation with temperature gradient

In the third step, a fully coupled THM simulation was performed. Initial conditions and the first steps of drift excavation and backfilling after one year are again the same as for the simulation at ambient temperature (Tab. 2.1), but since temperature and heat flux are introduced as additional degrees of freedom, temperature boundary conditions of 38.67 °C are already applied at the left and right boundaries (Fig. 2.3, left).

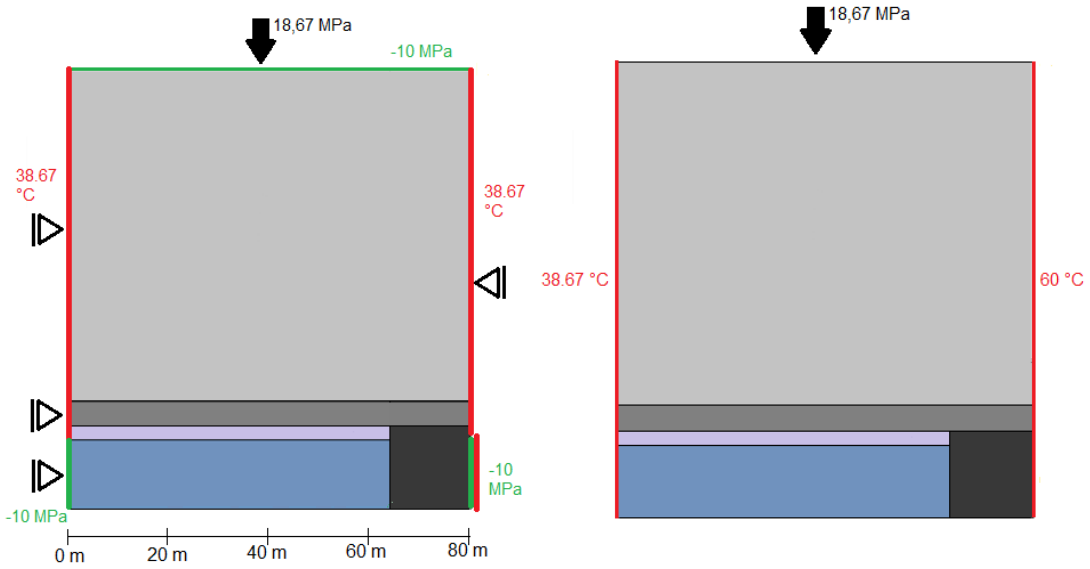

Fig. 2.3 Initial conditions for the THM coupled simulation (left), temperature conditions after two years simulation time (right)

After emplacement of the backfill (one year simulation time), another interval of one year is inserted during which the temperature condition at the right hand model side is raised to 60 °C. The temperature conditions after two years of simulation time are shown on the right side of Fig. 2.3. After another 100 years of simulation at dry conditions the hydraulic boundary conditions are changed in the same way as for the isothermal simulations (Fig. 2.4). Saturation is increased to 25 % at the left side of the backfill, and a seepage condition is applied at the right end of the salt concrete plug.

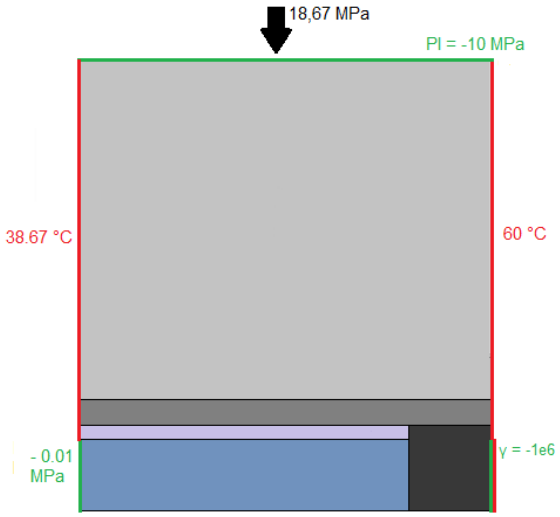

Fig. 2.4 Boundary conditions for the THM simulation after 102 years simulation time

3 Results

In this section, results of the different simulation variants are given in terms of porosity and saturation evolution at three locations in the backfill on the drift axis: 20 m, 40 m, and 60 m from the left hand model boundary (Fig. 2.2 and 2.3). Additionally, longitudinal sections are shown for certain time points.

3.1 Simulation at ambient temperature

Figure 3.1 shows the porosity evolution at three points in the backfill. All curves show the same trend: From year 1 until year 101 the porosity decreases as a consequence of the mechanical compaction process due to drift convergence. After year 101, a porosity of 17 % – 18 % is reached. Subsequently, the curve slope increases significantly because of the softening effect of the brine, enabling fluid assisted deformation. The minimum porosity of 1 % is reached after 180 years.

The higher porosity values of the green line at 60 m – when compared to the other two curves – are due to the support of the concrete plug which slows the compaction process in its vicinity. This effect becomes even more visible when plotting porosity along the drift axis (Fig. 3.2). The plug is located between 65 m and 80 m on the axis.

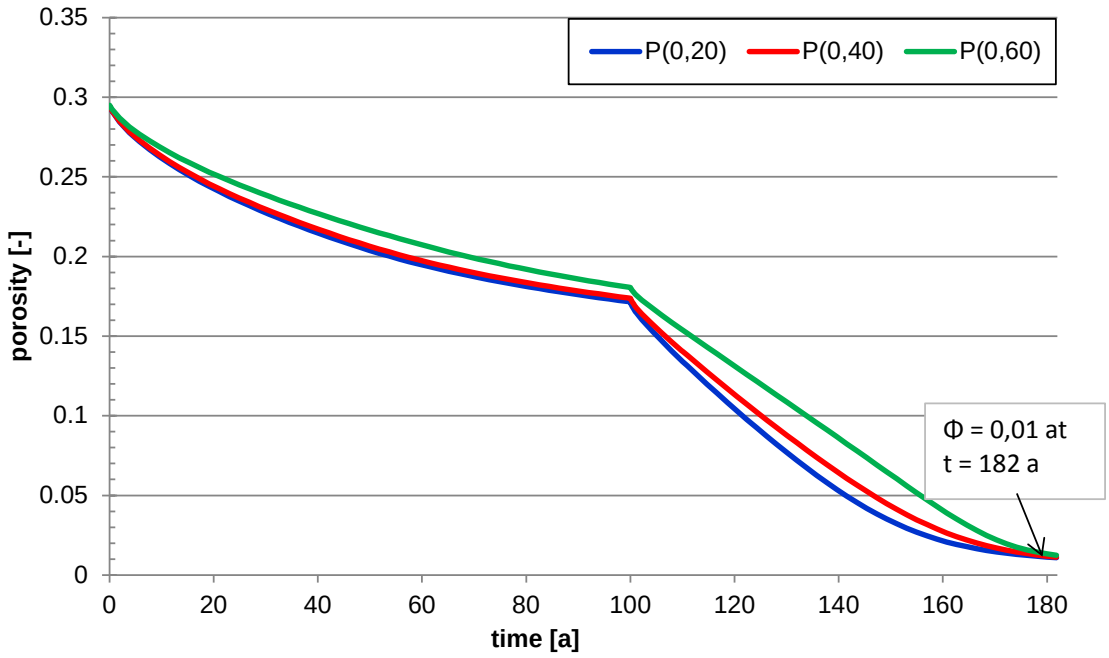

Fig. 3.1 Porosity evolution in the backfill – simulation at ambient temperature

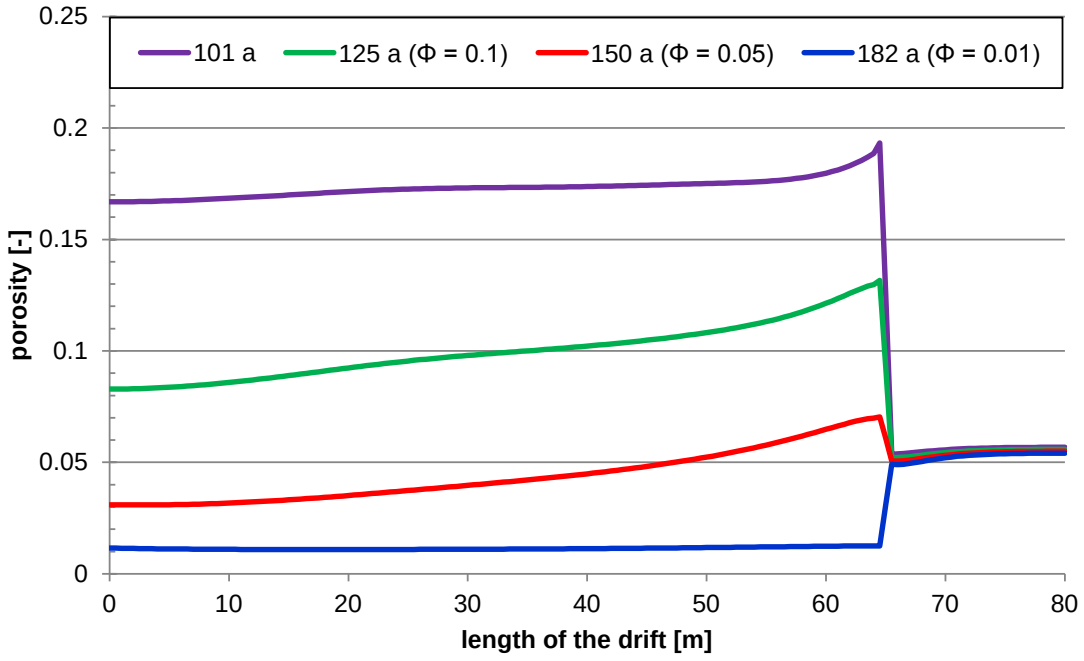

Fig. 3.2 Porosity distribution along the drift – simulation at ambient temperature

The liquid saturation evolution is shown in Fig. 3.3. Over the first 101 years there is no change in saturation because of the boundary condition. When brine enters the drift as a consequence of the increased saturation condition there is a rapid increase of saturation degree in all points, due to the high hydraulic conductivity. Then, the saturation de-

gree increases with time to a maximum of 100 % which is reached with the residual porosity of 1 % for the red and green curve. The blue curve at 20 m drift length remains at lower saturation. This is a result of the boundary condition: Since a saturation (and not a flux) boundary condition was applied, saturation close to the boundary cannot exceed the boundary value which 25 %. The longitudinal section (Fig. 3.4) shows that at minimum porosity – after 182 years – half the backfilled drift length is influenced by the boundary condition. The saturation in the salt concrete plug remains low because of its higher porosity and the seepage condition.

The saturation boundary condition with the open drift side was chosen for simplicity of the model. A more realistic model would include a plug with a seepage condition on the inflow side, or a flux boundary condition.

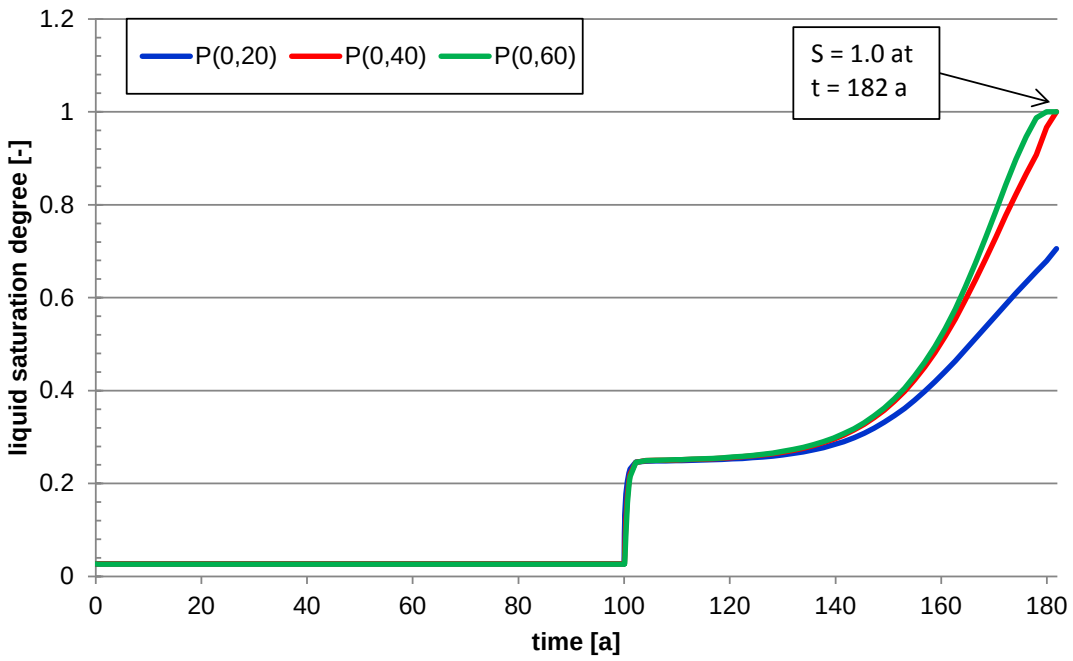

Fig. 3.3 Saturation evolution in the backfill – simulation at ambient temperature

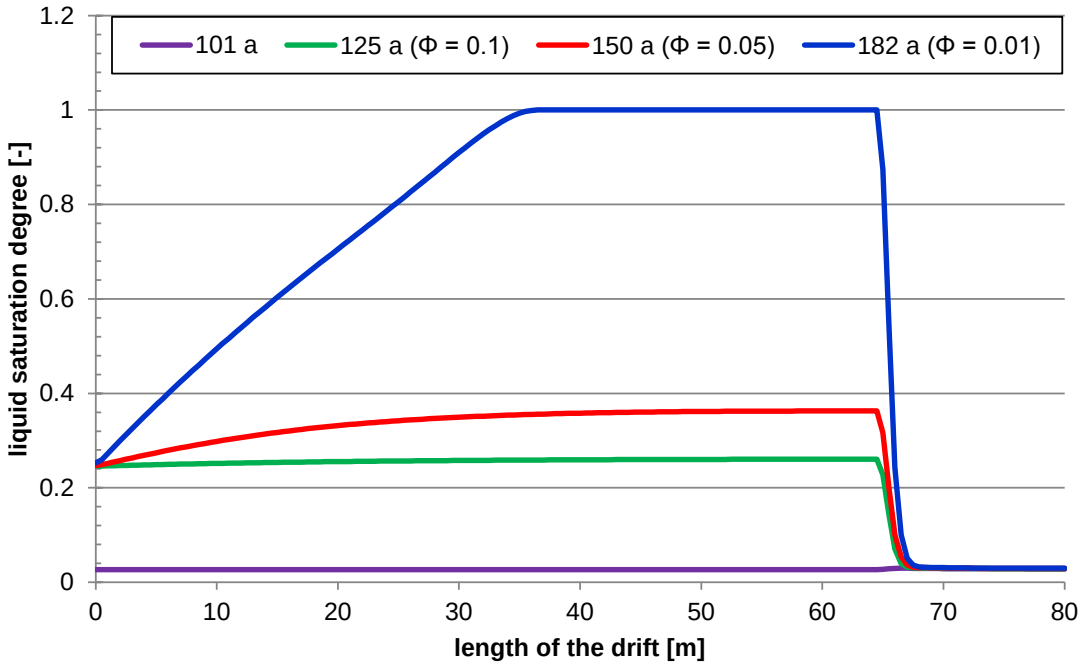

Fig. 3.4 Saturation distribution along the drift – simulation at ambient temperature

3.2 Simulation at constant elevated temperature

The porosity evolution at the three locations and the porosity distribution along the drift for various time points for the simulation at 60 °C are shown in Fig. 3.5 and Fig. 3.6, respectively. In comparison to the simulation at ambient temperature, compaction is considerably accelerated both for the dry and the wet period. During 100 years of dry compaction, already porosities of 6 % – 11 % are reached. After brine entry, only 19 years are required to reach the minimum porosity of 1 %.

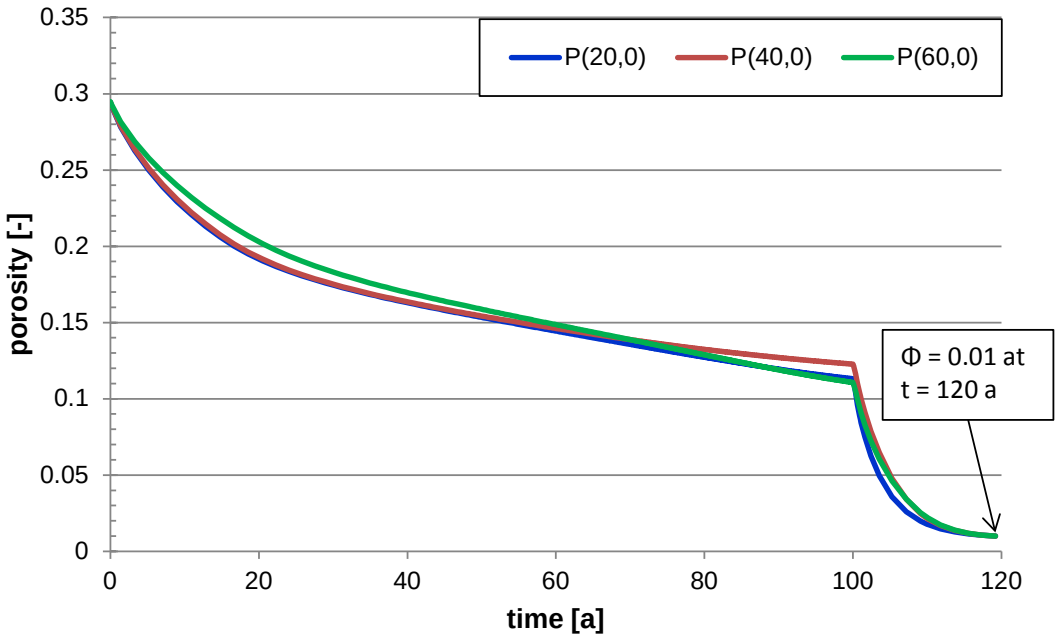

Fig. 3.5 Porosity evolution in the backfill – simulation at 60 °C temperature

The corresponding saturation evolution and saturation distributions along the drift are shown in Fig. 3.7 and Fig. 3.8, respectively. They are comparable to those of the simulation at ambient temperature with a time lapse effect, although Fig. 3.8 also shows that the porosity and related permeability after one year of brine inflow (102 years simulation time) have decreased far enough that the saturation boundary condition of 25 % is not immediately propagated through the backfill (green curve). Moreover, it shows that the influence of the saturation boundary condition on the saturation distribution reaches less far after reaching the minimum porosity, and the saturation at 20 m drift length actually reaches 100 % (blue curve).

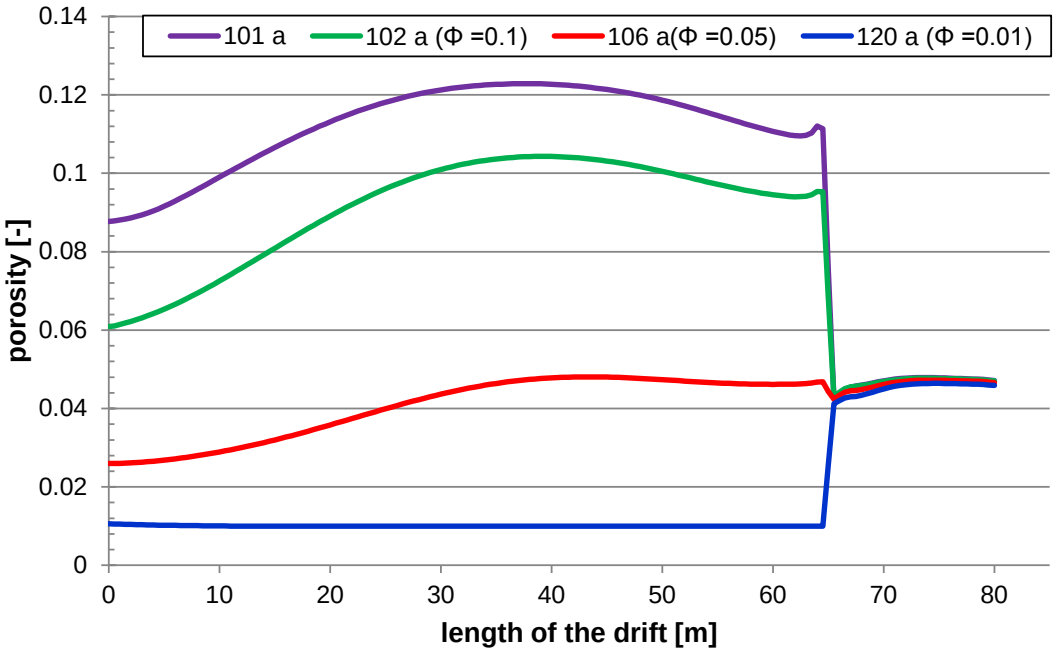

Fig. 3.6 Porosity distribution along the drift – simulation at 60 °C temperature

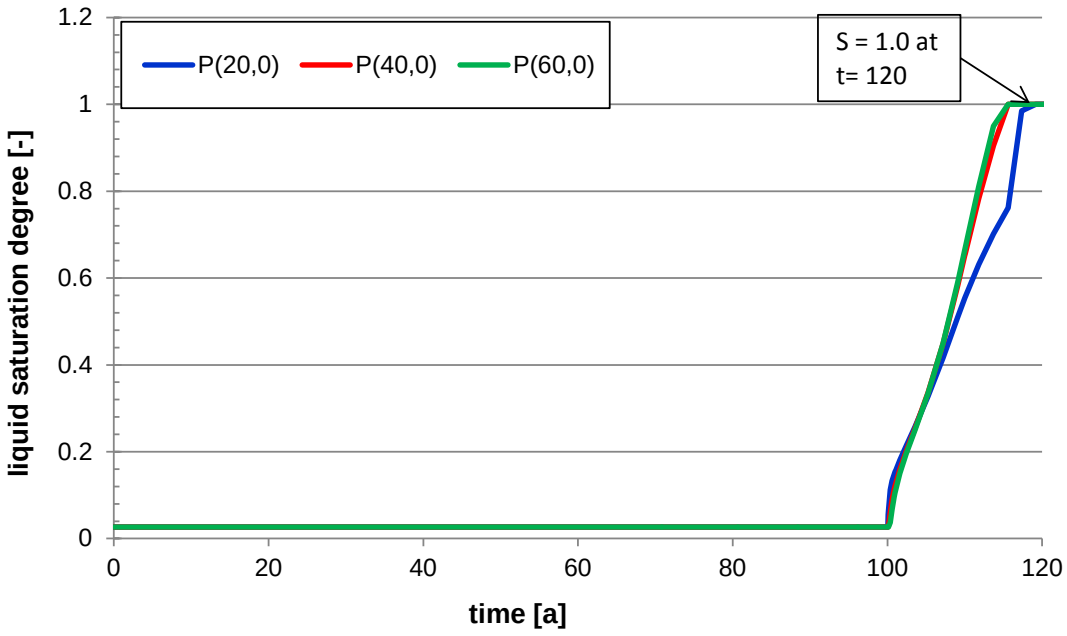

Fig. 3.7 Saturation evolution in the backfill – simulation at 60 °C temperature

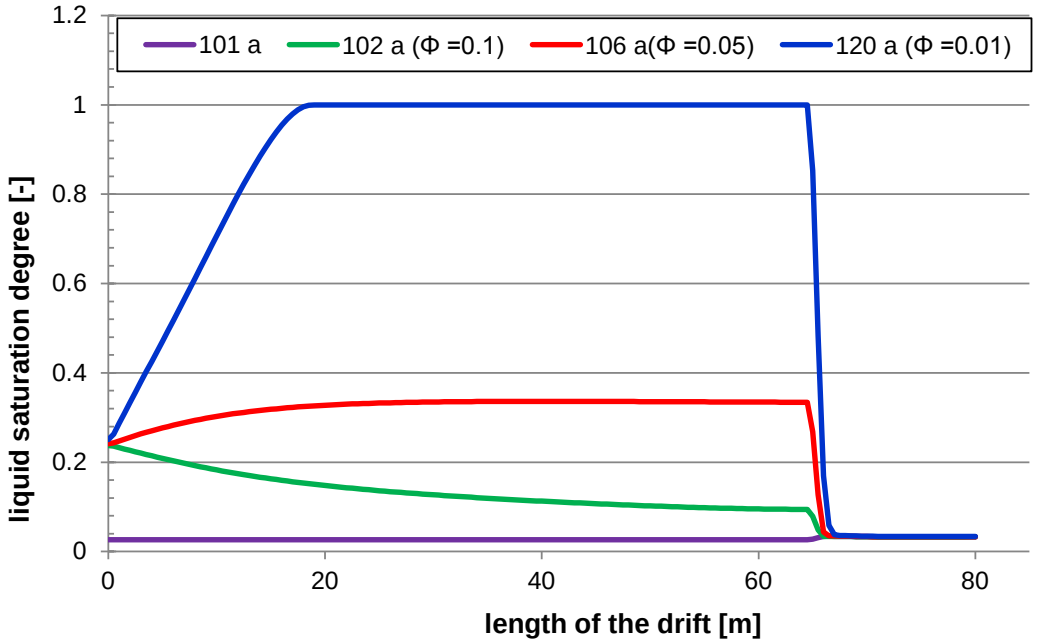

Fig. 3.8 Saturation distribution along the drift – simulation at 60 °C temperature

3.3 Fully coupled THM simulation with temperature gradient

For the fully coupled THM simulation, a temperature condition of 38.67 °C on the left model side and 60 °C on the right model side was applied. The temperature evolution at the three observation points in the drift is shown in Fig. 3.9. A steady-state temperature is reached at all points already during the dry compaction phase, after about 40 years. The temperature distribution in the model after reaching the steady state is shown in Fig. 3.10.

Since the first two simulations at constant temperature have shown a significant influence of the temperature level, it can be expected that the porosity evolution in this model with a spatially varying temperature will be different at the individual observation points. This is verified by Fig. 3.11. Especially in the dry compaction phase the three curves deviate more significantly from each other than in the isothermal simulations. Moreover, the porosity close to the plug shows the fastest decrease in porosity and the one close to the open drift side the slowest – as opposed to the other simulations, but in line with the temperature distribution. After brine inflow, the deviation diminishes, and all porosity curves quickly decrease to the minimum porosity.

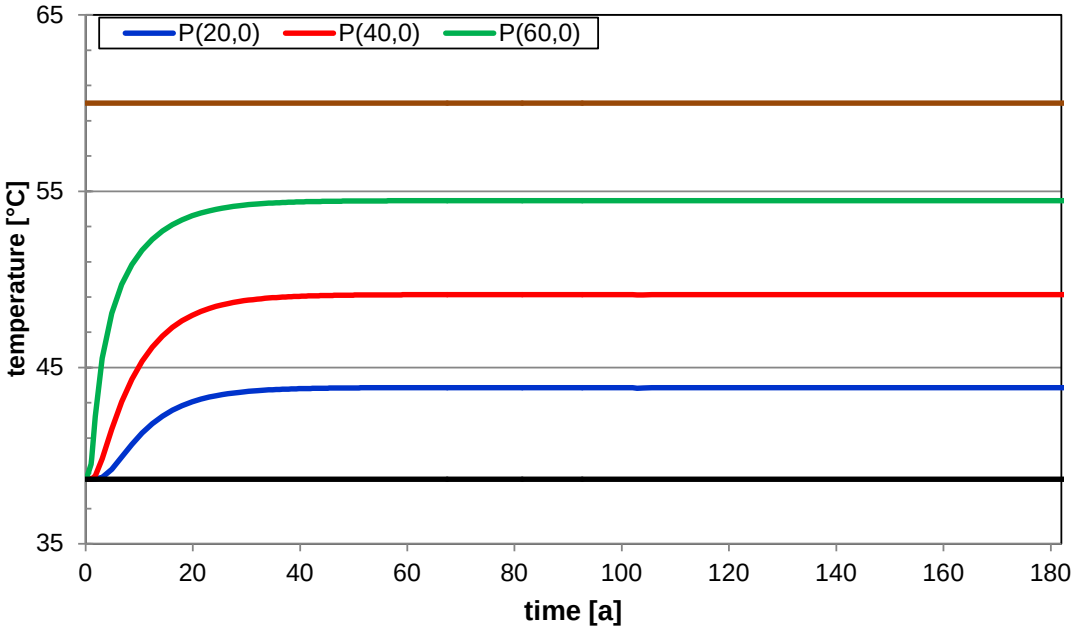

Fig. 3.9 Temperature evolution in the backfill – THM coupled simulation

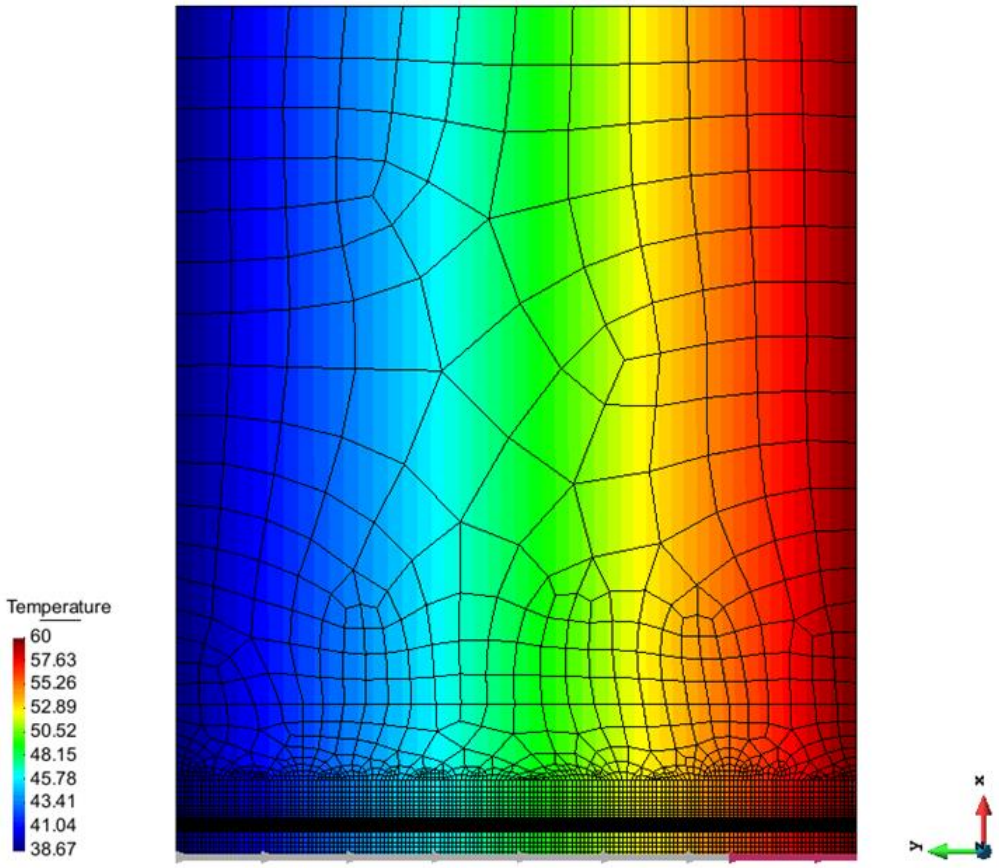

Fig. 3.10 Stationary temperature field – THM coupled simulation

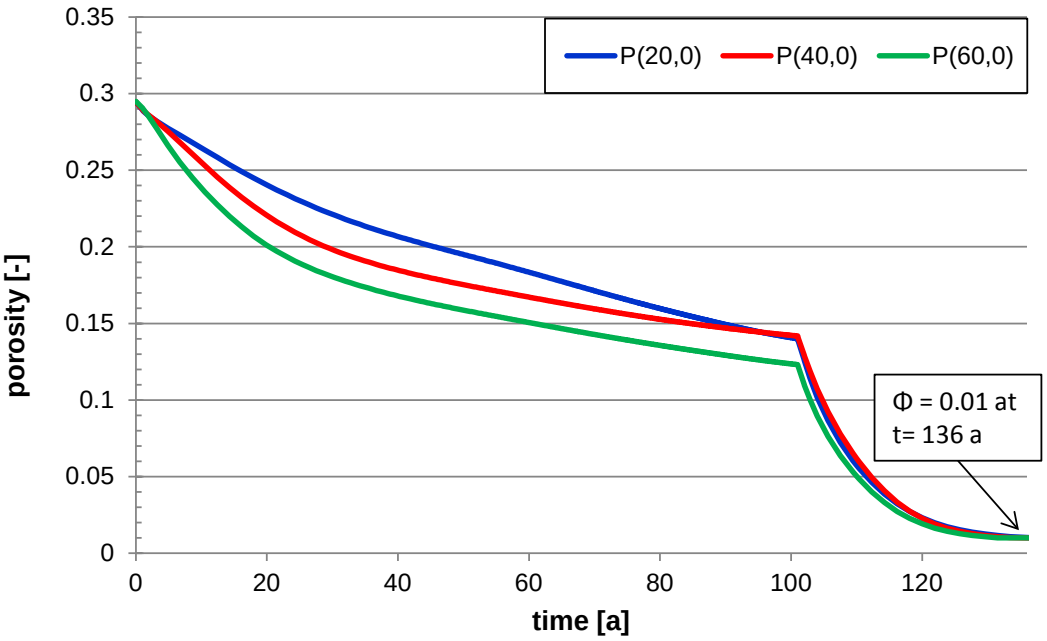

Fig. 3.11 Porosity evolution in the backfill – THM coupled simulation

Porosity distribution along the drift for several time points is shown in Fig. 3.12. the curves are bent much stronger than in the other simulations, as a result of the competing influences of temperature and support.

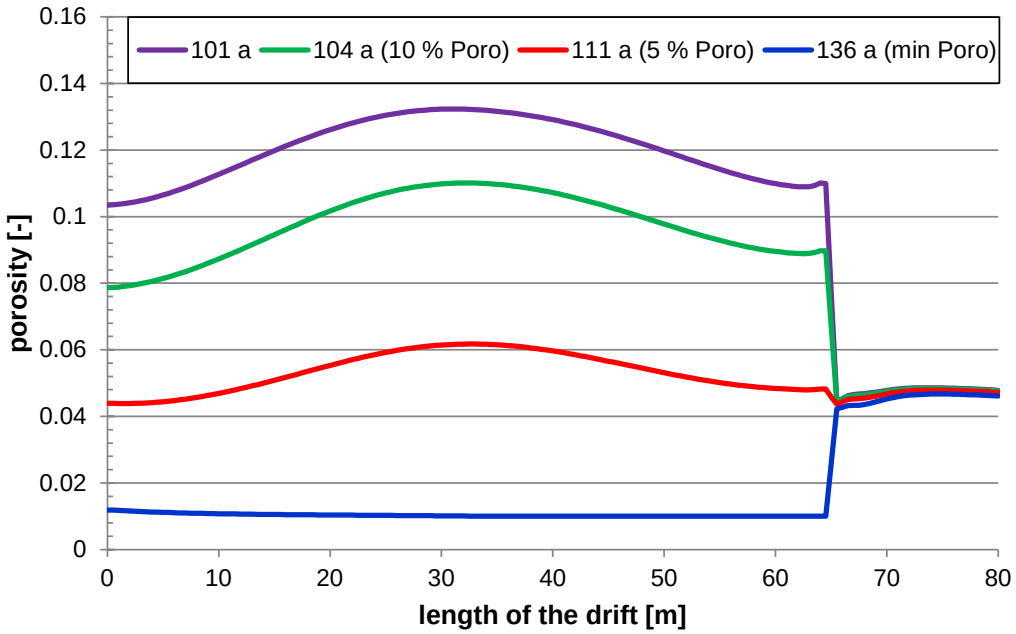

Fig. 3.12 Porosity distribution along the drift – THM coupled simulation

The saturation evolution and saturation distributions along the drift of the THM coupled simulation are shown in Fig. 3.13 and Fig. 3.14, respectively. In this simulation, the influence of the saturation boundary condition reaches again further into the drift.

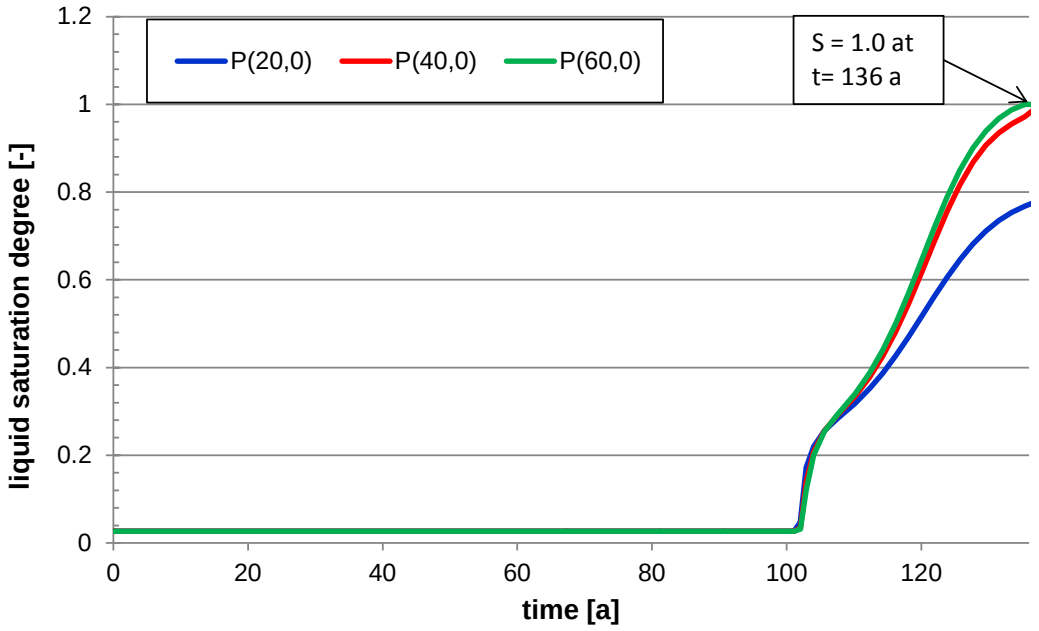

Fig. 3.13 Saturation evolution in the backfill – THM coupled simulation

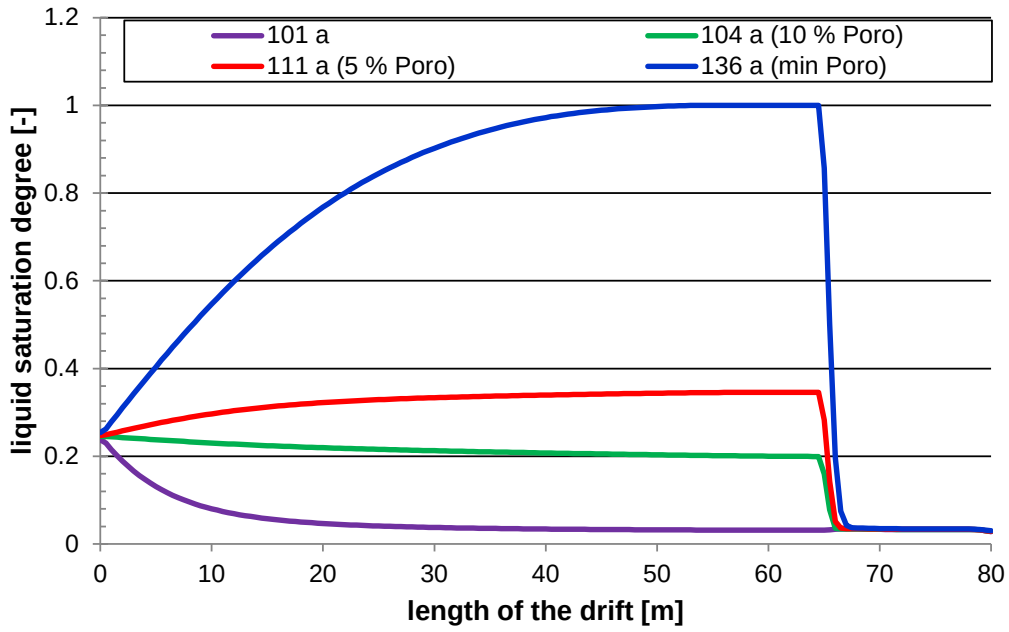

Fig. 3.14 Saturation distribution along the drift – THM coupled simulation

3.4 Comparison of different simulations

In this section, the evolution of porosity, saturation, and stress in the drift centre as obtained in the different simulations are plotted together for easier comparison.

Figure 3.15 shows the evolution of porosity. The increase of compaction rate with brine entry after 101 years (or 102 years in case of the THM coupled simulation) is clearly visible in all simulations. An increased temperature accelerates compaction both in the dry and wet phase, as can be seen when comparing the curves for ambient temperature and 60 °C. The THM simulation with temperature gradient results in a porosity curve running between the other two. This can be expected, because the temperature in the drift centre amounts to 49 °C in this simulation.

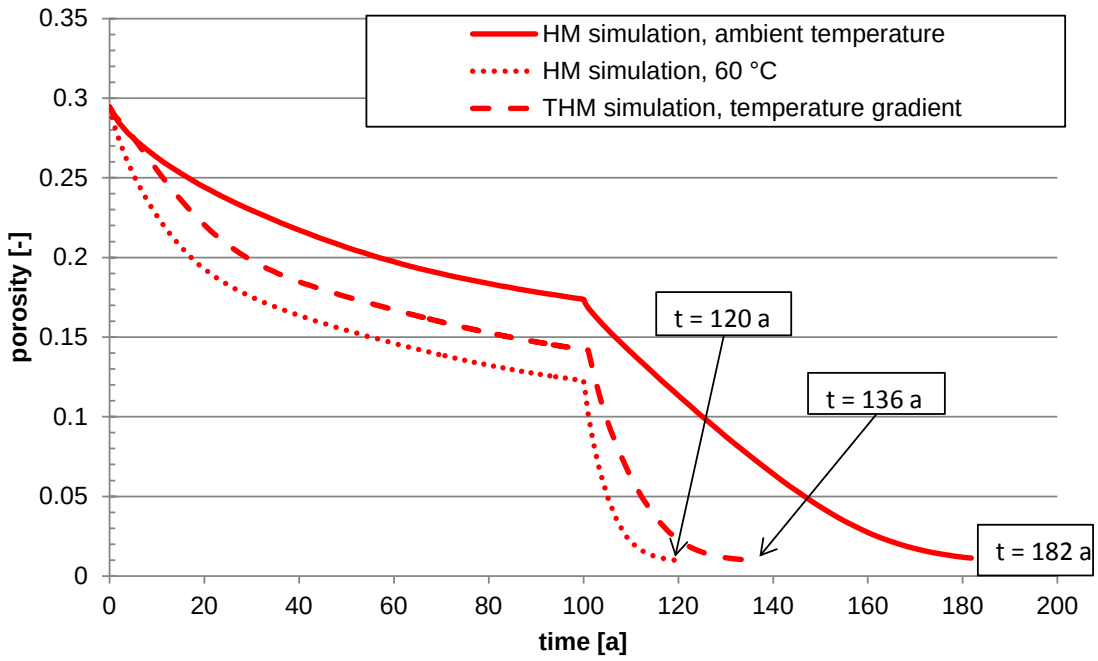

Fig. 3.15 Porosity evolution in the drift centre – comparison of different simulations

Saturation evolution is compared in Fig. 3.16. In the very early re-saturation phase, saturation in the ambient temperature simulation increases faster than for those with increased temperature. This can be explained by the higher porosity and related higher permeability of the backfill at the time of brine entry. Shortly afterwards, however, saturation in the warmer backfill rises much faster because of the accelerated porosity decrease.

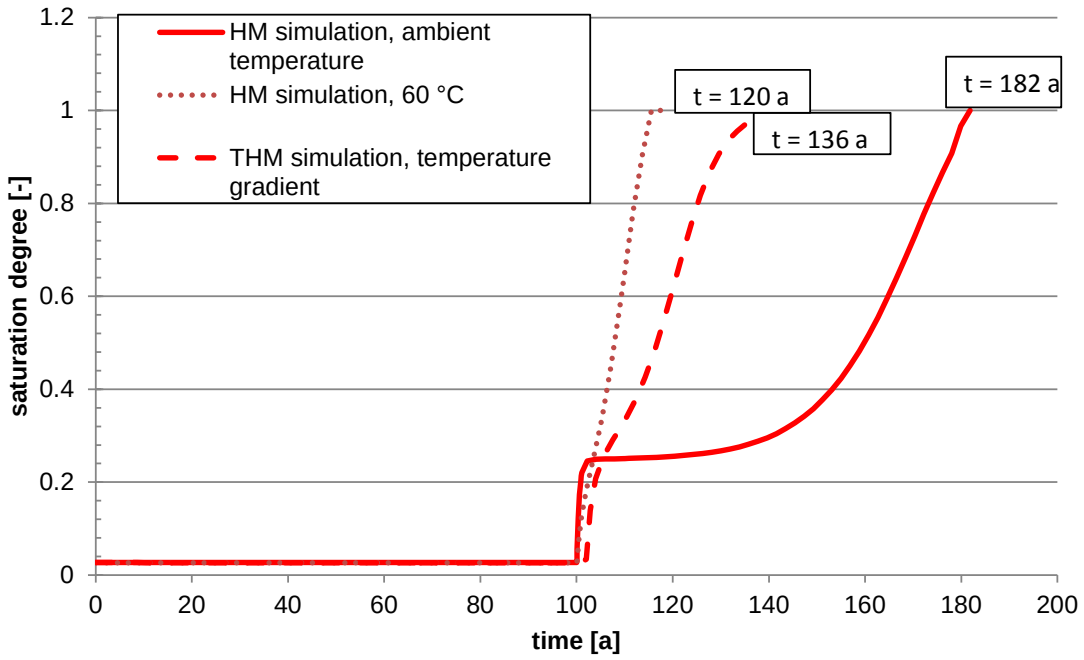

Fig. 3.16 Saturation evolution in the drift centre – comparison of different simulations

Both higher temperature and presence of brine result in a softening of the affected materials. While temperature affects both the backfill and the surrounding rock salt, mainly because of increased creep rates, the moisture effect is restricted to the crushed salt. Accelerated compaction is a result of a different stress-strain behaviour. This is illustrated by Fig. 3.17 which shows the evolution of minimum principal stress in the three simulations.

In the dry phase, minimum stress rises with time to nearly 6 MPa at ambient temperature, but to 11 MPa for the 60 °C case. This is explained by the fact that in the 60 °C case a significantly lower porosity is reached in the dry phase. The dry-phase end porosity of the ambient temperature case of 17.4 % is reached already after 31 years at 60 °C. This is a result of higher creep rates of the surrounding rock, so that a lower porosity is reached after 100 years.

Brine entry results in an instant softening of the backfill, visible by the sudden drop in all stress curves. With further compaction, stress in the backfill increases again with time. This happens faster again at higher temperature because of higher creep rates and faster compaction.

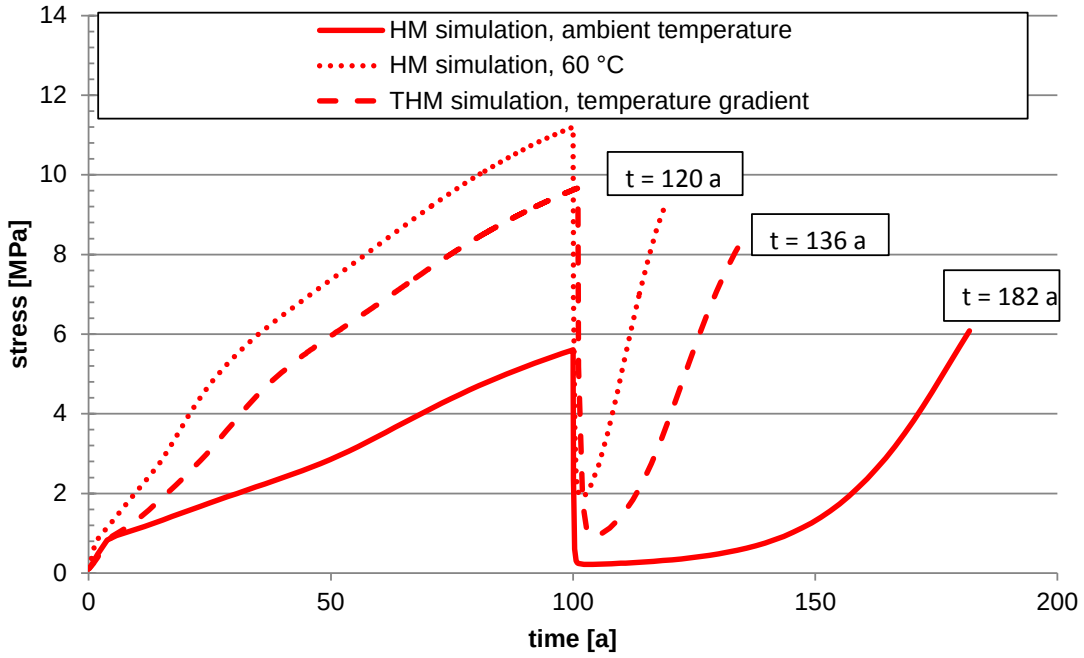

Fig. 3.17 Evolution of minimum principal stress in the drift centre – comparison of different simulations

4 Conclusions

The simulations have shown that the application of the available material models on a system of a backfilled drift leads to plausible and coherent results. Compaction of crushed backfill in a repository drift can in principle be modelled, both for the dry case and for a brine inflow, at constant or variable temperature. If it is possible to validate and calibrate the material models for crushed salt implemented in CODE_BRIGHT, it has a high potential for the prediction of the THM behaviour of a repository in rock salt.

References

/COD 10/ CODE-BRIGHT User's Guide, Departament d'Enginyeria del Terreny, Cartogràfica i Geofisica, Universitat Politècnica de Catalunya (UPC), 2010.